physica status solidi

pss

www.pss-journals.com

reprint

WILEY-VCH

Phys. Status Solidi A, 1–8 (2012) / **DOI** 10.1002/pssa.201127617

physica status solidi a
www.pss-a.com
applications and materials science

Electron microscopic imaging of an ion beam mixed SiO_2/Si interface correlated with photo- and cathodoluminescence

H.-J. Fitting*[,1], L. Fitting Kourkoutis[2], B. Schmidt[3], B. Liedke[3], E. V. Ivanova[4], M. V. Zamoryanskaya[4], V. A. Pustovarov[5], and A. F. Zatsepin[5]

[1] Physics Department, University of Rostock, Universitätsplatz 3, 18051 Rostock, Germany
[2] School of Applied and Engineering Physics, Cornell University, Ithaca, NY 14853, USA
[3] Research Center Dresden-Rossendorf, Institute of Ion Beam Physics, POB 510119, 01314 Dresden, Germany
[4] Ioffe Physico-Technical Institute, Polytekhnicheskaya ul. 26, St. Petersburg 194021, Russia
[5] Department of Physics and Technology, Ural Federal University, ul. Mira 19, Ekaterinburg 620002, Russia

Received 20 October 2011, revised 6 February 2012, accepted 22 February 2012
Published online 16 March 2012

Keywords cathodoluminescence, energy-filtered TEM, ion beam mixing, silicon suboxides

* Corresponding author: e-mail hans-joachim.fitting@uni-rostock.de, Phone: +49 381 498 6760, Fax: +49 381 498 6802, Web: web.physik.uni-rostock.de/elektronen/

Energy filtered transmission electron microscopy (EFTEM), scanning transmission electron microscopy (STEM) imaging, and electron energy loss spectroscopy (EELS) of a thin 28 nm SiO_2 layer on Si substrate implanted by Si^+ ions with an energy of 12 keV are reported. The maximum concentration of implanted Si^+ ions is located near the SiO_2–Si interface region leading there to an ion beam mixed gradual SiO_X ($2 \geq x > 0$) buffer region, which is even extended into the Si substrate by atomic collisions (knocking-off and knocking-on processes) during ion implantation. Thus, the width of this SiO_X buffer layer amounts to about 30 nm extended from 10 to 40 nm depth. The SiO_X profile is demonstrated by the above given electron microscopic and spectroscopic methods. Thermal annealing leads to partial phase separation from SiO_{X1} to SiO_{X2} with $x_2 > x_1$ and silicon precipitates (partially nc-Si) changing the photo- (PL) and cathodoluminescence (CL) spectra especially in the near IR-region, probably, due to the formation of Si nanoclusters and associated quantum confinement effects.

1 Introduction Implantation induced self-organizing processes are an important investigation in nanotechnology research. Usually self-organizing processes result in the formation of low-dimensional structures at surfaces, interfaces as well as in the bulk of semiconducting, dielectric, and insulating materials, *e.g.*, by means of ion implantation and subsequent thermal treatment. The relevance of such research is based on the need to find new approaches that are linked with the development and fabrication of quantum-size electronic devices.

In optoelectronic and photonic applications based on modern silicon CMOS technology the formation, distribution, and stabilization of nanostructures in thin dielectric SiO_2 layers as well as at the interface to the silicon substrate are still under investigation [1].

Adding optical functionality to a silicon microelectronic chip, however, is one of the most challenging problems of materials research. This could be possible using silicon itself, in the form of quantum dots dispersed in a silicon dioxide matrix. Their net optical gain is of the same order as that of direct-bandgap quantum dots [2]. Commonly these layers are produced from under-stoichiometric silicon-rich oxide (SRO) SiO_X ($x < 2$) thin films or by additional Si-ion implantation [3, 4], thermal evaporation of silicon or silicon monoxide under partial oxidation in ambient oxygen atmosphere [5, 6] or by plasma-enhanced chemical vapor deposition (PECVD) [7]. Under-stoichiometric SiO_X systems have been used as initial material to obtain thin silica layers with different concentrations of embedded silicon nanocrystals by means of thermal annealing at temperatures 700–1300 °C [8–12] and respective phase separation. The main intention was to develop light-emitting silicon-based luminescence devices [13]. On the other hand, amorphous silicon nanostructures occur as precipitated phase in

thermally treated stoichiometric SiO_2 samples even at low annealing temperatures [10]. Moreover, it is well known that under-stoichiometric silicon oxide SiO_X ($x \leq 2$) undergoes thermal decomposition. In Ref. [14], we have proposed the following reactions:

(i) The ion implantation of Si into stoichiometric SiO_2 leads to a non-stoichiometric SiO_{X1}:

$$SiO_2 + \left(\frac{2}{x_1} - 1\right) Si \rightarrow \frac{2}{x_1} SiO_{X1}. \quad (1)$$

(ii) This SiO_{X1} may undergo partial phase-separations to SiO_{X2} with $x_2 > x_1$ and aggregated Si atoms:

$$SiO_{X1} \rightarrow \frac{x_1}{x_2} SiO_{X2} + \left(1 - \frac{x_1}{x_2}\right) Si. \quad (2)$$

(iii) Even, a total phase separation into stoichiometric silica and silicon may be assumed during subsequent annealing [10]:

$$SiO_{X2} \rightarrow \frac{x_2}{2} SiO_2 + \left(1 - \frac{x_2}{2}\right) Si. \quad (3)$$

Finally, Eq. (3) is a reverse reaction of Eq. (1).

In previous papers soft X-ray emission spectroscopy (SXES) [15] and X-ray photoelectron spectroscopy (XPS) [16] studies of the same charge of Si^+ ion implanted SiO_2/Si interfaces are presented and discussed. A strong valence band (VB) transformation was observed due to the formation of the under-stoichiometric SiO_X buffer layer with significant structural re-arrangements demonstrated by the volume-sensitive XES [15]. In surface-sensitive XPS spectra a triple VB sub-structure appears due to strongly hybridized Si 3d3s–O 2p electronic states [16]. Thus, the XPS spectra demonstrated an oxygen depletion in the surface layer.

In the present paper electron microscopic imaging and electron energy loss spectroscopy (EELS) of the Si^+-implanted SiO_2/Si heterostructures are reported in order to examine the principal possibility of Si-nanoparticle formation in these gradual heterostructures SiO_X with $2 \leq x \leq 0$, *i.e.*, from silica SiO_2 to pure crystalline c-Si.

2 Experimental n-Type (001)Si-wafers are oxidized in dry oxygen until they possess a stoichiometric oxide layer SiO_2 of about (20–30) nm proven by ellipsometry. These samples are of microelectronic quality and have been implanted by Si^+ ions with an energy of 12 keV and an ion fluence of 10^{16} cm^{-2} using conventional ion implantation carried out at the Ion Beam Center of the Research Center Dresden-Rossendorf (Germany), see *e.g.*, Ref. [4]. At this implantation energy the spatial maximum of the implanted Si^+ ion concentration of 7 at% is located around the depth of 20 nm in front of the original interface, here at 28 nm depth, see Fig. 1.

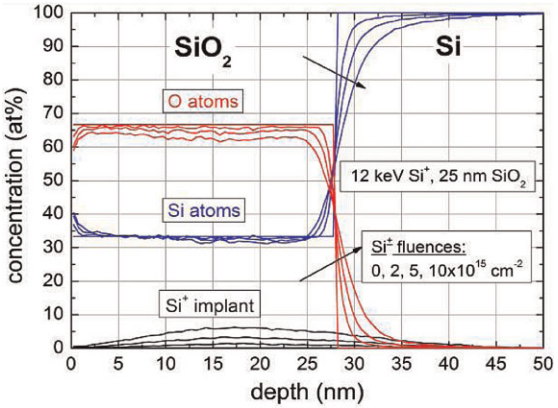

Figure 1 (online color at: www.pss-a.com) TRIDYN simulation of the ion beam mixing process showing the Si^+ implantation profile and the variation of Si and O atom concentrations across the SiO_2/Si sample with an original interface at a depth of 28 nm.

The final atomic concentration profile was calculated by the computer simulation tool TRIDYN including sputtering and swelling processes as well as interface mixing developed by Möller and Eckstein [17]. This program is based on the sputtering version of the TRIM program for multicomponent targets. A Monte Carlo (MC) code is applied to compute range profiles of implanted ions, composition profiles of the target, and sputtering rates for a dynamically varying target composition [18]. It takes into account compositional changes both due to the spatial distribution of target atoms deposited in collision cascades, and due to the presence of the implanted ions. The local density of the target is allowed to relax according to a given function of the densities of the individual components. The application of the program covers a wide range of problems like the collisional atomic mixing of multilayered targets, dynamic implantation profiles at large ion fluences, and the fluence-dependent preferential sputtering of multicomponent materials.

In Fig. 1 the atomic concentration profiles of implanted Si^+, and the natural constituents silicon Si and oxygen O are presented in dependence of the sample depth. In the non-treated sample SiO_2/Si we see a sharp interface at a depth of 28 nm from the expected 33 at% Si and 67 at% O toward pure Si of the substrate. The Si^+ implantation profile is shown at the bottom of Fig. 1 with a maximum concentration of 7 at% around 20 nm for the given ion influence of 10^{16} cm^{-2}. Obviously, increased ion fluences produce increased ion beam mixing and formation of SiO_X, with $x < 2$ on the oxide side and $x > 0$ on the Si substrate side. The transition becomes gradual within a wide zone between 10 and 40 nm, *i.e.*, a width of about 30 nm. While on the oxide side a formation of SiO_X with a stoichiometry of $1 \leq x < 2$ can be expected, on the substrate side an oxide with a stoichiometry of $0 < x < 1$ is indicated. In the first case, $x \geq 1$, we will expect the phase separation into SiO_2 and Si nanoclusters according to Eqs. (1)–(3). Within the substrate, with a stoichiometry of $x < 1$, we can expect the phase transition according to Eq. (2) into a-Si and SiO_{X2} nanoclusters and

amorphous a-Si, the more, as in this region beyond the previous interface the oxygen incorporation prevails the silicon implantation rate, as clearly shown in Fig. 1. Moreover, beneath the SiO_2 surface down to 3 nm we recognize an oxygen deficit, due to preferential sputtering of O-atoms into vacuum during Si^+ ion implantation, see also the XPS results in Ref. [16].

Thus, we can conclude that the current mode of Si^+ implantation leads to the appearance of an ion beam mixed interface buffer layer, consisting of a gradual non-stoichiometric SiO_X matrix with $2 \geq x \geq 0$ and, probably, of Si precipitates and Si nanoclusters (nc) near the interface between the SiO_2 and the c-Si substrate.

Such a SiO_X interface transition was made visible by EELS and annular dark field scanning transmission electron microscopy (ADF-STEM) [19]. The authors used the EELS losses of the electronic states O-K and Si-$L_{2,3}$ (as in the present work). There the interface transition in a non-implanted very thin a-Si–SiO_2–c-Si sample occurs very abruptly over 1–2 atom layers. On the other hand, in Si^+ implanted thick (500 nm) SiO_2 layers the Si cluster growth during subsequent thermal annealing has been made visible by energy filtered transmission electron microscopy (EFTEM) and tomography using the Si (17 eV) and SiO_2 (23 eV) plasmon losses for EFTEM, [14]. Si clusters of 1–5 nm size at a concentration of 1.5×10^{18} cm^{-3} embedded in an under-stoichiometric SiO_X matrix became visible. This means that some kind of ion-beam mixing associated with processes of self-organization and cluster growth by Ostwald ripening occur.

In the present paper the structure and bonding across the SiO_X buffer layer will be studied using EFTEM, spatially resolved EELS and STEM performed on a 200 keV FEI Tecnai F20 TEM/STEM. The electron transparent sample was prepared using mechanical tripod polishing followed by a short, low angle, low energy ion-milling cleaning step, see also Ref. [14].

The respective luminescence measurements were carried out in a special cathodoluminescence (CL) spectrometer in the Ioffe Institute (St. Petersburg). It is extended to near infrared (NIR) wavelengths of 1550 nm (0.8 eV) with a high resolution of 0.2 nm (0.02 eV) and a special photoelectron-multiplier (PMT 83) for NIR detection [20]. However, for the weak luminescence of SiO_2 we used a lower resolution of 5 nm (0.01 eV). The control of this spectrometer and of the electron beam is done on the basis of a CAMAC microanalysis system.

Further on VUV photoluminescence (PL) and photoluminescence excitation (PLE) spectra were measured on the SUPERLUMI station of HASY-LAB/DESY in Hamburg/Germany under excitation by pulsed synchrotron radiation at temperatures of 9–10 K and 287 K. The luminescence spectra were obtained using an ARC Spectra Pro-308i monochromator and an R6358 P photomultiplier (Hamamatsu). The luminescence spectra were measured with a wavelength resolution of $\Delta\lambda = 3.2$ Å. More details see in Ref. [21].

3 Results and discussion In EFTEM the structure was imaged with inelastically scattered electrons in a narrow energy range. To enhance the contrast from the implanted Si a 4 eV energy slit was centered on the Si plasmon peak, Fig. 2. It was one aim of the present work to visualize collective electronic effects of SiO_X by EFTEM fixed on the Si plasmon peak at 17 eV. Obviously, in Fig. 2 there appears a clear contrast change between SiO_X ($x > 1$) and SiO_X ($x < 1$) at about 28 nm as well as to pure Si at about 40 nm.

No lattice fringes were observed in this layer and convergent electron beam diffraction (CBED) confirmed the layer to be amorphous. To study the chemistry and the bonding of the system spatially resolved EELS was performed in STEM mode. A narrow electron beam was scanned along a line across the interfaces and an electron energy loss spectrum was recorded at each point. By integrating across the Si-L and the O-K edges the Si and O concentration profiles were obtained, as shown in Fig. 3. At the SiO_2/Si interface the concentration profiles show a transition region, where the Si concentration gradually increases to the value in Si. This region corresponds to the expected SiO_X buffer layer. This is further confirmed by analyzing the Si-L edge fine structure variations across the layer as shown in Fig. 4. The Si-L edge fingerprints for SiO_2 and c-Si are distinct and well known. In the buffer layer the Si-L edge fine-structure transitions from SiO_2 to a-Si is observed, see Ref. [22] for an EELS fine structure database. A drastic change can be recognized near a depth of 30 nm, however, only over a distance of about 5 nm when SiO_X changes from $x > 1$ to $x < 1$.

The structure of the system was further studied using STEM imaging. By varying the detector angles, the imaging conditions can be switched from high-angle annular dark field (HAADF) to low-angle annular dark field (LAADF). To

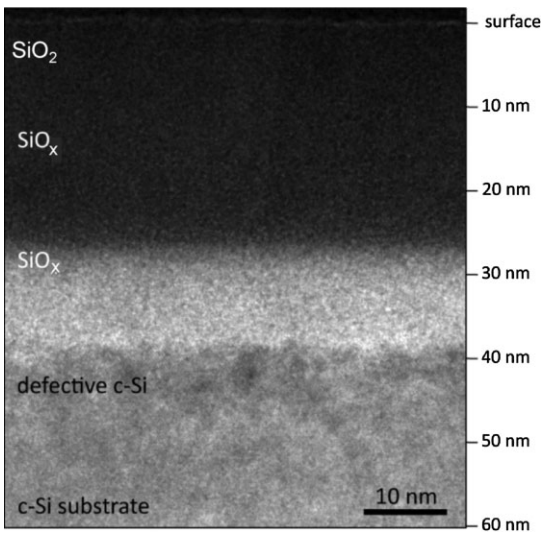

Figure 2 Energy filtered (EF) TEM image of the ion-beam mixed SiO_X buffer layer at the SiO_2/Si interface. A 4 eV energy slit was centered on the Si plasmon peak at 17 eV to demonstrate the different SiO_X zones.

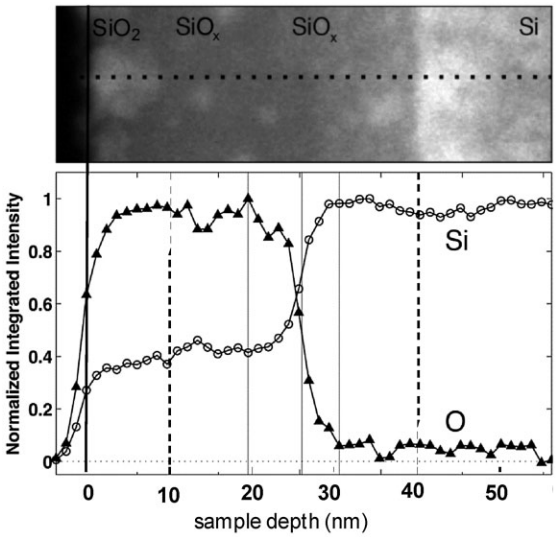

Figure 3 Silicon (Si-L) and oxygen (O-K) concentration profiles across the SiO_2/SiO_X/Si structure measured by spatially resolved EELS performed in an STEM. The dotted line in the LAADF STEM image (top) indicates where the profile was measured; the dotted lines in the bottom part show the SiO_X buffer layer zone in the widest range and in comparison to Fig. 1.

a first approximation, HAADF images are determined by chemical contrast. Due to channeling of the electron probe in crystalline material the contrast can, however, strongly be modified. Similarly, atomic disorder in the crystal can lead to a reduced contrast by dechanneling off of the atomic column.

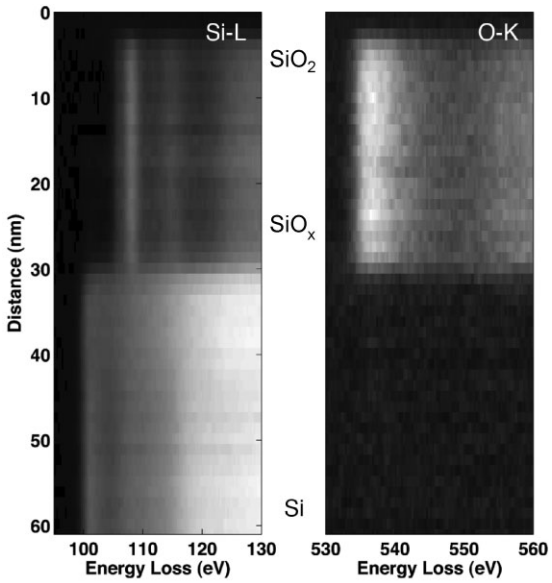

Figure 4 Evolution of the Si-L and O-K edge fine structure across the layers shown in Fig. 3. The large differences between the characteristic Si-L edge fine structure of c-Si and SiO_2 are apparent. The Si-L edge fine structure in the buffer layer shows a transition from SiO_2 to amorphous Si.

In LAADF imaging additional contrast can arise from strain fields at interfaces, grain boundaries and around defects [23, 24]. Figure 5 shows a comparison of the HAADF and the LAADF image of the SiO_2/buffer layer/Si system. Dark patches in the HAADF image below the buffer layer suggest that this region of the Si substrate is defective, which is most likely caused by the implantation process. This defective layer is also clearly visible in the high magnification EFTEM image of Fig. 6. The LAADF image shows a bright layer at the buffer layer/Si substrate interface. Similar contrast has been previously observed at the a-Si/c-Si interface [23]. The strain field around the defects can give rise to additional contrast in the LAADF image.

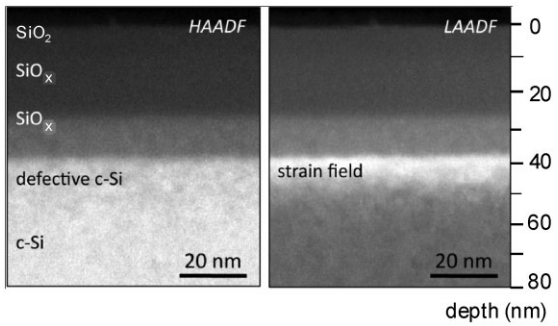

Figure 5 High angle (HA) and low angle (LA) ADF STEM images of the structure. Dark patches in the HAADF image below the buffer layer suggest that this region of the Si substrate is defective, which is most likely caused by the implantation process. The LAADF shows additional strain contrast at the buffer layer/Si substrate interface.

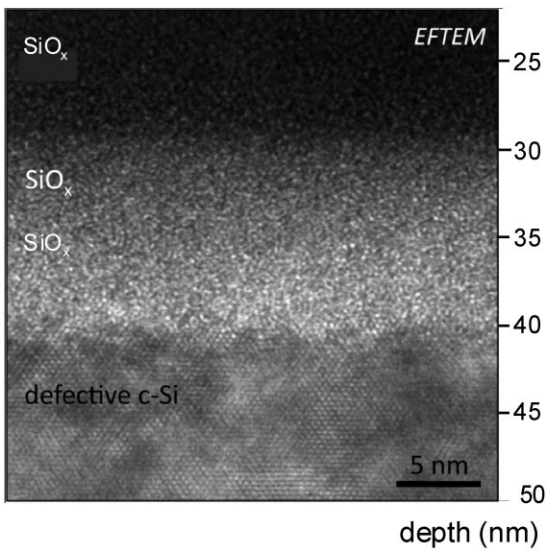

Figure 6 High magnification EFTEM image of the ion-beam mixed SiO_X buffer layer at the SiO_2/Si interface. As in Fig. 2, a 4 eV energy slit was centered on the Si plasmon peak. Lattice fringes are visible in the Si substrate, however, the fringe contrast is reduced or missing in patches directly below the buffer layer suggesting that this layer is defective.

After rapid thermal annealing (RTA) the EFTEM image in Fig. 7 shows a more rapid transition from the SiO_X region to the Si substrate beginning in the original interface near 30 nm. However, in the Si^+ implanted zone between 10 and 30 nm one may recognize small silicon clusters with diameters less than 4 nm as we have observed previously in Si^+ implanted silica SiO_2:Si^+, see [14, 27]. Quantum confinement with changes of the electronic structure of nanoclusters will be observed at cluster sizes below 3 nm in diameter. However, the EELS signal at the 17 eV Si plasma frequency simply increases when crossing an Si cluster. Thus, it is recorded by EELS signal intensity and not by a peak shift. In Ref. [14], the EELS spectra of SiO_2 and SiO_X with 1.9 are compared! They show already a clear difference in intensity. Thus, all EFTEM images are done with a 4 eV window around the 17 eV plasma frequency.

The zones of non-stoichiometry SiO_X, of defects, and lattice strains should strongly affect the PL and CL spectra as already shown in Ref. [14]. Commonly, CL emission spectra of pure SiO_2 are identified with particular defect centers within the atomic network of silica including the nonbridging oxygen-hole center (NBOHC): =Si–O(–) ... (+)Si= associated with the red luminescence band R at 650 nm (1.9 eV) and the oxygen deficient centers (ODC): =Si–Si= with the blue B (460 nm; 2.7 eV) and ultraviolet UV band (290 nm; 4.3 eV), respectively [25]. In Si doped SiO_2 the ODC blue emission is increased as has been shown already in Ref. [14] and additional emission bands are observed in the green–yellow region G (560 nm, 2.2 eV) caused by Si atom agglomeration up to Si nanoclusters.

On the other hand, the wide extend of the NBOHC red band R (1.85 eV) in Fig. 8 into the NIR region may indicate additional luminescence centers of silicon aggregates as found in Si^+ ion implanted thick (500 nm) SiO_2 layers, see Refs. [14, 27]. Indeed, when resolving the R band shoulder by a high spectral resolution we find a side-band shifted

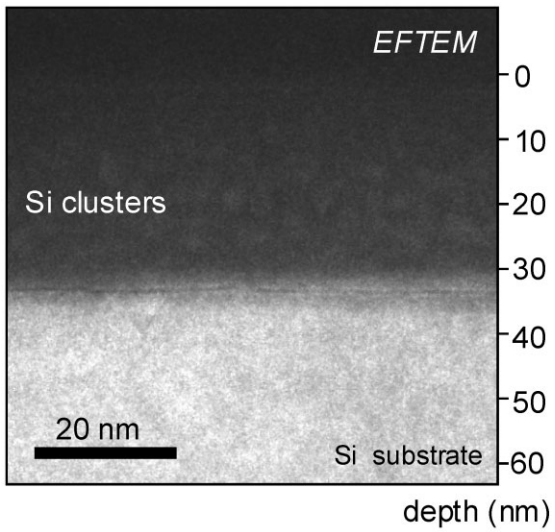

Figure 7 Si^+ implanted sample after thermal annealing; Si nanoclusters (nc) are observed between 10 and 30 nm depth within the former SiO_X buffer layer with $x > 1$, followed by a soft transition zone with $x < 1$ down to 40 nm to pure Si ($x = 0$), recorded for the Si plasmon peak.

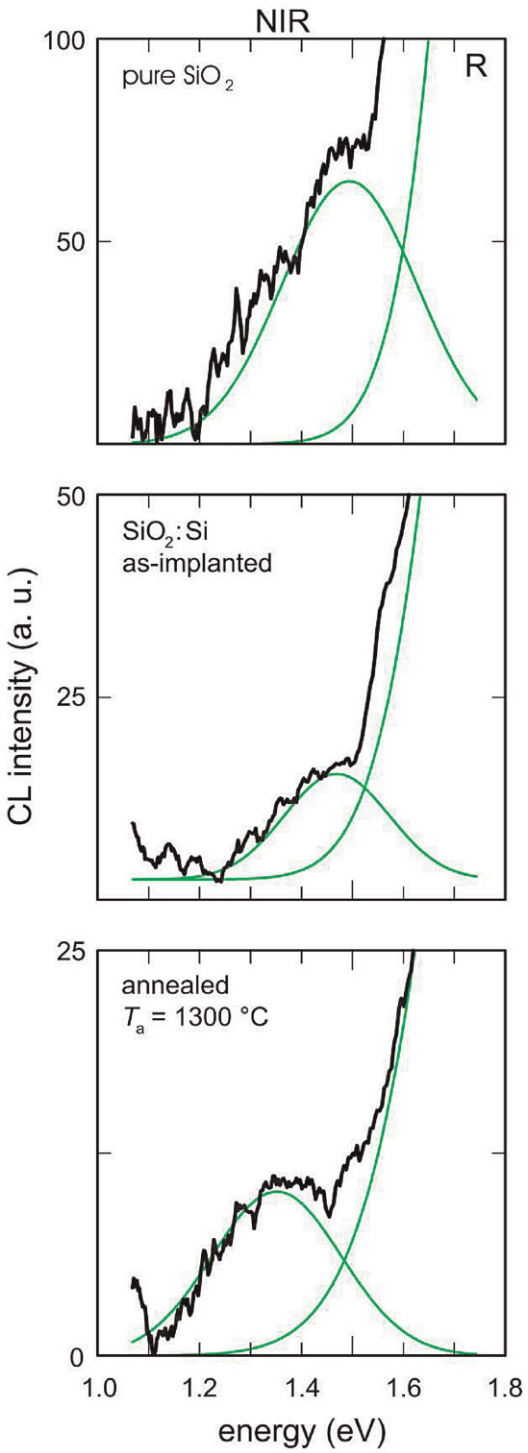

Figure 8 (online color at: www.pss-a.com) NIR CL spectra of a thick (500 nm) SiO_2:Si layer, see Ref. [14], in dependence on the annealing temperature T_a showing the red band R (1.85 eV) with a side band moving to lower energies with T_a; electron beam excitation: $E_0 = 2.5$ keV; $j_0 = 0.9$ A/cm^2.

toward NIR with increasing annealing temperature T_a of the implanted sample SiO_2:Si^+, Fig. 8. We observe an initial side-band with a position at 1.5 eV for pure SiO_2, 1.45 eV for the as-implanted sample, and at lower energy 1.35 eV for the thermally annealed sample at $T_a = 1300\,^{\circ}C$. The lower luminescence energies may indicate the increasing Si cluster growth and their approach toward bulk Si. The bulk Si features will be obtained already at cluster sizes of about 5 nm [14].

Also in the present paper the ion beam mixed layers have been investigated by luminescence spectroscopy. For that reason the electron beam excitation for CL in the 20 nm SiO_2/Si heterostructure is demonstrated by an MC simulation, Fig. 9. For the given incident electron beam energy $E_0 = 1.5$ keV the depth of maximum excitation is positioned around the maximum implantation zone in 20 nm depth. Thus, we will get an optimum CL signal from the SiO_X buffer layer up to a depth of 35 nm. The respective CL spectra are presented in Fig. 10; for the NIR region on the left and for the visible (vis) region on the right hand side in Fig. 10. The vis spectra (right) show the main bands in SiO_2 and its suboxides, also called SROs: R (1.85 eV), G (2.2 eV), and B (2.7 eV) which we find well developed for the non-implanted SiO_2/Si sample. In Ref. [26] we could show that this typical luminescence band structure appears for silica suboxides SiO_X with a stoichiometric factor $x > 1.5$. After Si^+ implantation a wide band over the full visible region (1.8–3.0 eV) dominates the spectra with a maximum in the green–yellow region (2.1 eV). RTA annealing leads again to silica-like spectra but now with a dominating blue B-band at 2.65 eV.

A similar spectra change due to implantation and RTA annealing is obtained for the NIR spectra, Fig. 10 (left). Here, a broad band around 1.25 eV (992 nm) is shown, probably, due to amorphous silicon formations, [27]. After Si^+ ion implantation this band becomes sharper and is shifted to 1.35 eV (918 nm). This spectra region is typical for Si nanoclusters, with diameters less than 4 nm, appearing in a SiO_X matrix [10–12, 27]. After RTA annealing these clusters mostly have grown to a more extend and reach diameters above 4 nm, thus this band shifts again to the longer wavelengths and lower energies 1.15 eV (1078 nm) approaching the spectra of bulk crystalline c-Si [27].

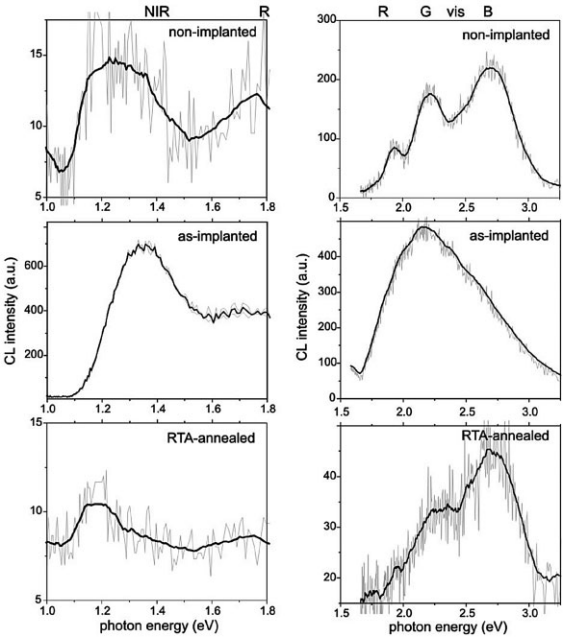

Figure 10 CL spectra ($E_0 = 1.5$ keV) in the NIR (left) and visible region (vis) (right) showing the typical Si band around 1.2 eV before Si^+ implantation and appearing again after RTA annealing. The "as-implanted" sample shows a very broad band with a maximum around 1.35 eV, probably, due to quantum confinement of low-dimensional nanoclusters with various size (left). The vis spectra (right) demonstrate the three main SiO_2 bands: red R (1.85 eV), green–yellow G (2.2 eV), and blue B (2.65 eV) where the G-band dominates in the as-implanted and highly disordered sample.

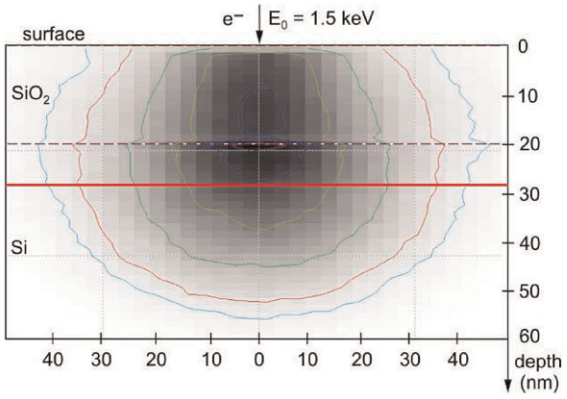

Figure 9 (online color at: www.pss-a.com) MC simulation of CL excitation with $E_0 = 1.5$ keV electrons; thus the maximum excitation zone lies in the implantation maximum depth 20 nm, still near the Si/SiO_2 interface at 28 nm.

A comparison with PL and high energy excitation by synchrotron radiation (13.8 eV, 90 nm) is presented in Fig. 11. Here, as expected, the red R (1.85 eV) and the blue B (2.65 eV) bands appear in the non-implanted sample. Obviously, the B band is highly broaden and, probably, includes parts of the green band G (2.2 eV). After RTA annealing we observe a contrary effect: the B band becomes much sharper while the red band B seems to take over parts of the green band G, *i.e.*, this sub-band G should been shifted toward lower energies. According to Ref. [25], both the B and the G bands are ODC and should indicate the Si agglomeration too. So we were looking to the PLE spectra in Fig. 12. For excitation of the blue B band, appearing here at 2.67 eV there are relative maxima around 5.1 eV, well-known as ODC defect excitation, [25], as well as at 10.5 and 11.8 eV. Obviously, these high energy excitations are band–band transitions in the SiO_X matrix.

4 Conclusions After high fluence Si^+ ion implantation into and around the interface of a thin 20 nm a-SiO_2

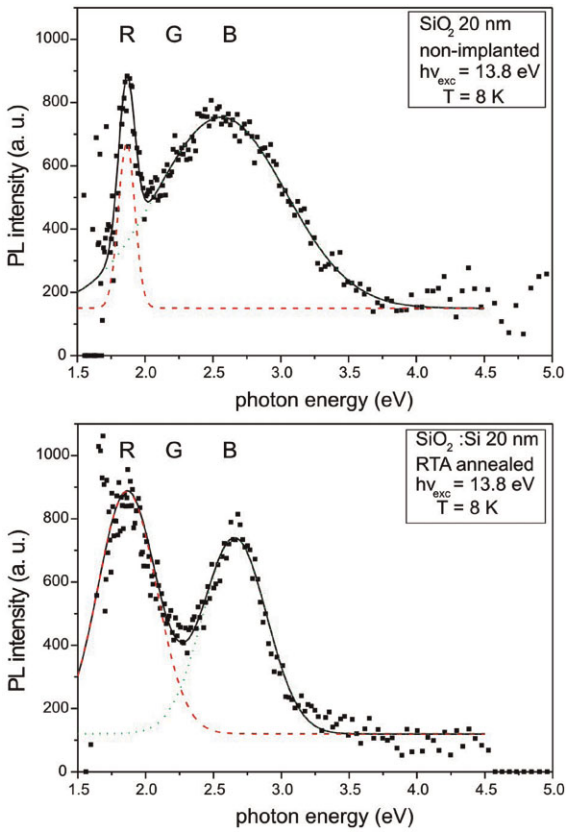

Figure 11 (online color at: www.pss-a.com) VUV-synchrotron radiation (13.8 eV) excited PL showing the red NBOHC (1.85 eV) and the blue ODC (2.65 eV) luminescence.

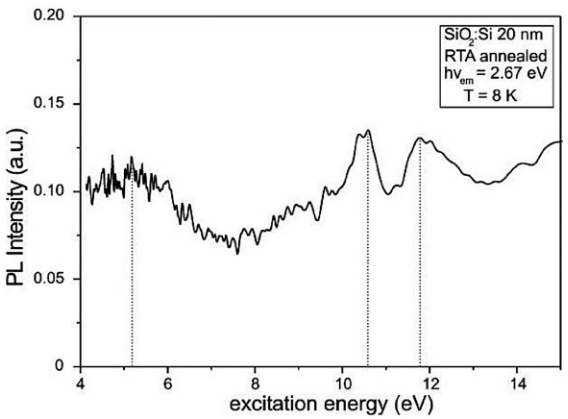

Figure 12 VUV PLE spectroscopy for the blue B ($h\nu_{em} = 2.65$ eV) luminescence band (ODC) showing relative excitation maxima at $h\nu_{exc} = 5.1$, 10.5, and 11.7 eV.

layer on a c-Si substrate the formation of an ion-beam mixed buffer layer SiO_x in this region was imaged by EFTEM/STEM microscopy and compared with TRIDYN computer simulations. This structure modulation is due to atomic knock-off and knock-on effects and respective ion beam mixing processes during the high-fluence Si^+ ion implantation into the interface region. Thus, the buffer layer SiO_X is extended over about 30 nm, even extended 10 nm into the previously crystalline Si substrate followed by a highly defective (probably amorphized) Si zone of about 10 nm. The buffer layer consists mainly of a gradual understoichiometric SiO_X matrix with decreasing x toward and into the Si substrate.

The CL and PL spectra in the visible (vis) region show the typical silica defect bands R, G, B but with changing weighting after Si^+ implantation and after RTA thermal annealing. In the NIR region sub-bands appear between the NBOHC band R at 1.85 eV and that of amorphous silicon at 1.2 eV shifting to lower energies with thermal annealing. Thus we may conclude that they are associated with growing Si nanoclusters in the SiO_X matrix finally confirmed by EFTEM imaging in Fig. 7.

References

[1] Y. Ishikawa, N. Shibata, and S. Fukatsu, Thin Solid Films **294**, 227 (1997).
[2] L. Pavesi, L. Dal Negro, C. Mazzoleni, G. Franzo, and F. Priolo, Nature (London) **408**, 440 (2000).
[3] T. Shimizu-Iwayama, D. E. Hole, and I. W. Boyd, J. Phys.: Condens. Matter **11**, 6595 (1999).
[4] H.-J. Fitting, T. Barfels, A. N. Trukhin, B. Schmidt, A. Gulans, and A. von Czarnowski, J. Non-Cryst. Solids **303**, 218 (2002).
[5] S. Hayashi and K. Yamamoto, J. Lumin. **70**, 352 (1996).
[6] U. Kahler and H. Hofmeister, Opt. Mater. **17**, 83 (2001).
[7] M. Zacharias, L. X. Yi, J. Heitmann, R. Scholz, M. Reiche, and U. Gösele, Solid State Phenom. **94**, 95 (2003).
[8] F. Iacona, G. Franzò, and C. Spinella, J. Appl. Phys. **87**, 1295 (2000).
[9] D. Nesheva, C. Raptis, A. Perakis, I. Bineva, Z. Aneva, Z. Levi, S. Alexandrova, and H. Hofmeister, J. Appl. Phys. **92**, 4678 (2002).
[10] M. Zacharias, J. Heitmann, R. Scholz, U. Kahler, M. Schmidt, and J. Bläsing, Appl. Phys. Lett. **80**, 661 (2002).
[11] L. X. Yi, J. Heitmann, R. Scholz, and M. Zacharias, Appl. Phys. Lett. **81**, 4248 (2002).
[12] D. Hiller, S. Goetze, F. Munnik, M. Jivanescu, J. W. Gerlach, J. Vogt, E. Pippel, N. Zakharov, A. Stesmans, and M. Zacharias, Phys. Rev. B **82**, 195401 (2010).
[13] S. Ossicini, L. Pavesi, and F. Priolo, Light Emitting Silicon for Microphotonics, Springer Tracts Mod. Phys. **194**, 123 (2003).
[14] H.-J. Fitting, L. Fitting Kourkoutis, R. Salh, M. V. Zamoryanskaya, and B. Schmidt, Phys. Status Solidi A **207**, 117 (2010).
[15] D. A. Zatsepin, S. Kaschieva, M. Zier, B. Schmidt, and H.-J. Fitting, Phys. Status Solidi A **207**, 743 (2010).
[16] D. A. Zatsepin, P. Mack, A. E. Wright, B. Schmidt, and H.-J. Fitting, Phys. Status Solidi A **208**, 1658 (2011).
[17] W. Möller and W. Eckstein, Nucl. Instrum. Methods Phys. Res., B **2**, 814 (1984).
[18] W. Möller, W. Eckstein, and J. P. Biersack, Comp. Phys. Commun. **51**, 355 (1988).

[19] D. A. Muller, T. Sorsch, S. Moccio, F. H. Baumann, K. Evans-Lutterodt, and G. Timp, Nature **399**, 758 (1999).
[20] M. V. Zamoryanskaya, S. G. Konnikov, and A. N. Zamoryanskii, Instrum. Exp. Tech. **47**, 477 (2004).
[21] A. F. Zatsepin, H.-J. Fitting, V. S. Kortov, V. A. Pustovarov, B. Schmidt, and E. A. Buntov, J. Non-Cryst. Solids **355**, 61 (2009).
[22] For a selection of EELS reference spectra see www.weels.net.
[23] Z. Yu, D. Muller, and J. Silcox, J. Appl. Phys. **95**, 3362 (2004).
[24] L. Fitting, S. Thiel, A. Schmehl, J. Mannhart, and D. A. Muller, Ultramicroscopy **106**, 1053 (2006).
[25] G. Pacchioni, L. Skuja, and G. L. Griscom, Defects in SiO_2 and Related Dielectrics: Science and Technology, NATO Science Series (Kluver, Dordrecht, 2000).
[26] R. Salh, A. von Czarnowski, M. V. Zamoryanskaya, E. V. Kolesnikova, and H.-J. Fitting, Phys. Status Solidi A **203**, 2049 (2006).
[27] R. Salh, L. Fitting, E. V. Kolesnikova, A. A. Sitnikova, M. V. Zamoryanskaya, B. Schmidt, and H.-J. Fitting, Semiconductors **41**(4), 381 (2007).

